Benjamin Karlsen
Lars Roar Sætran

Cross-sectional wake measurements of actuator disks.

June 2019

NTNU
Norwegian University of
Science and Technology

NTNU
Norwegian University of
Science and Technology

Cross-sectional wake measurements of Actuator disks.

Benjamin Karlsen[1] and Lars Roar Saetran[1]

1. Department of Energy and Process Engineering, NTNU

Correspondence: Lars Roar Saetran (lars.satran@ntnu.no)

1 Abstract

1.1 *English*

The cross-sectional wake normal to the flow of two non-rotating wind turbine models has been measured at $x = 4D$ downstream. By using a 4 hole Cobra probe we have extended normal flow measurements to get three-dimensional information about the wake. The technique has been validated against hot wire measurements for mean flow values and turbulence intensity, proving the probes ability to measure turbulence accurately. The cross-section of the wakes revealed how both disks experienced significant downwash, meaning the wake center was not located at the geographical center of the disk. The velocity components $\langle v \rangle$ and $\langle w \rangle$ showed the mechanism of this, directing the flow downward and towards the center of the disk. The vertical components showed in both cases an area with strong downwards velocity in the upper regions of the wake. The comparison of the two disks revealed large differences with the wire disk having an undeveloped wake with a larger velocity deficit in the center, while the spider web disk had a wider wake with a lower central velocity deficit. The turbulent statistics Ti and Reynolds shear stresses, $\langle u'v' \rangle$, $\langle u'w' \rangle$, showed how the turbulence had reached the center of the spider web disk, regenerating the wake at a much higher rate than seen in the wire disk. Lastly, the wire disk and spider disk were compared with cross hot wire measurements of a wind turbine wake. The wire disk showed good agreement with slightly lower turbulence values, while the spider web disk showed a very different velocity profile and much higher turbulence levels. These results prove that the choice of actuator disk is of crucial importance when modeling turbine wakes.

1.2 *Norsk*

Eit tversnitt normalt på straumninga i vakane til to ikkje-roterande vindturbinmodellar har blitt målt ved $x = 4D$ nedstraums. Ved å bruke ein 4-hols Cobra probe har vanlege aksiale straumningsmålingar blitt utvida til å gi tre-dimensjonal informasjon om straumninga. Målemetoden har blitt samanlikna med hot wire målingar for middelverdier og turbulens intensitet, so har vist probene sin evne til å måle turbulens med høg presisjon.

Tversnittet av vakene viste at begge diskane opplevde nedoverretta avbøying av straumningen, noko som betyr at vake senteret ikkje var ved det vertikale midtsenteret til diskane. Hastighetskomponentande, $\langle v \rangle$ og $\langle w \rangle$ viste korleis straumninga var retta nedover og mot senteret av vaken. Dei vertikale målingane viste eit område med ein sterk nedoverretta hastighet i øvre delen av vaken for begge diskane, noko som retta straumninga nedover. Samanlikninga av dei to diskvakane viste stor skilnad, der vaierdisken hadde ein uutviklet vake med ein lavare aksial hastighet, medan edderkoppdisken hadde ein breiare vake, med høgare hastighet i vakesenteret. Turbulens intensitet Ti og Reynolds skjærspenningar viste korleis turbulensen hadde nådd senteret i vaken på edderkopp disken, noko som regenererte vaken med ein mykje høgare rate enn i vaierdisken. Tilslutt vart vaier-, og edderkoppdiskvakane samanlikna med ein roterande turbinvake. Vaierdisken viste god semje med turbinen, med litt lågare turbulensverdiar, medan edderkoppdiskvaken viste ein veldig annleis fartsprofil og mykje høgare turbulensverdiar. Resultata viser at valet av aktuatordiskmodell er svært viktig når ein modellerer turbinvaker.

2 Introduction

In wind farms, front row turbines extract energy from the incoming wind. This creates a wake with velocity deficit and increased turbulence which becomes the inlet condition of back row turbines. These turbines are known to produce less power (Barthelmie et al., 2010) and have shorter lifespan caused by dynamic loads induced by the turbulent wake (Tian et al., 2014). Therefore knowledge about the wake is of high importance when planning wind farms layout in order to make proper production and maintenance predictions.

Several different methods are used, ranging from analytical wake models to Computational Fluid Dynamics (CFD) and experimental testing (Vermeer et al., 2003). Of these the simplest, most cost efficient is to use analytical models of the wake, solving for conservation of mass and momentum (Crespo et al., 1999). However, these are based on assumptions like the existence of a self-similar wake state independent of its origin (Jensen, 1983), (Bastankhah and Porté-Agel, 2014). Also, the use of empirically calibrated equations from specific field measurements means they are subject to limitations (Kermani et al., 2013).

To calculate the wake characteristics with better accuracy, more advanced methods are needed. CFD solves the 3-D Navier Stokes equations which represent the wake flow with better accuracy (Vermeer et al., 2003). Because of the high computational cost of solving turbulence down to the lowest scale, for industrial purposes, one has to rely on turbulence modeling using the Reynolds-Averaged Navier Stokes(RANS) equations. The turbine is modeled as a momentum sink using the Actuator Disk (AD) principle, matching the momentum loss to the given turbines thrust coefficient (Hansen, 2013). Many different AD models exist, the simplest use a uniform force extraction, while more advanced can add things like radial loading, rotation or

tip vortexes (Mikkelsen, 2003). The more advanced models, however, require knowledge about the turbines airfoil which is often confidential information (Stergiannis et al., 2017). Ignoring the physics of a turbines energy extraction, the goal of these methods is to replicate the far wake characteristics of the turbine wake, where rotor effects have diminished and downstream turbines are placed. A measurement campaign of turbine wakes by Bartl and Saetran (2016a) was compared with CFD using the simplest AD model and several different RANS models (Stergiannis et al., 2017). This showed that most of the turbulence models using the AD overestimated the near wake turbulence generated which caused the AD wake to regenerate faster than found in the experiments.

It has been of interest to test experimentally what the consequences of neglecting the rotor have on the wake. Several different porous disks have been used to this extent. Saetran and Pierella (2017) studied the wakes of two different wooden disks. One using a monoplane grid, and the other a biplane grid, showed intrinsically different flow pattern. The biplane grid, despite its axisymmetric shape, created an asymmetric wake. Aubrun (2007) showed that by playing with the solidity of several different uniformly meshed wire disks, any velocity deficit could be reproduced. Further experiments showed the ability to reproduce even higher order statistics when comparing uniformly meshed wire disks with rotating turbines in atmospheric boundary layer conditions (Aubrun et al., 2013). Experiments with similar disks, using stereo particle image velocimetry (PIV), giving three component flow measurements, was conducted by Lignarolo (2015). This showed good overlap in the wake expansion of the wire disk compared to the turbine. The largest differences were seen in the near wake turbulence where the turbines tip vortexes were still present. Camp and Cal (2016) tested the porous disk concept and compared with turbines in a 4x3 turbine setup using PIV. The actuator disk model had a decreasing radial blockage meant to equal the blockage caused by a turbine. This showed the largest differences in the near wake of both mean kinetic energy and also of the vertical mean kinetic energy flux $\langle u'v'\rangle U$ but was reduced in the far wake regions to 3% and 16% respectively.

In this experimental work, two different porous disks have been used with the same solidity of $\sigma = 57\%$. A metal wire disk (WD) with a uniform mesh, based on a design of Aubrun (2007) was used to model the simplest actuator disk with a uniform thrust on the flow. Also, an acrylic plastic disk was used. The disk had a radially decreasing solidity, shaped like a spider web disk(SD), based on a design by Camp and Cal (2016). The drag coefficients of the disks were measured on a force balance showing Reynolds number independence. To get information about all three flow components a TFI (TFI, 2019) Cobra Probe (CP)was used. The CP was compared with pitot tube and hot wire(HW) data (Kyrkjeboe, 2019) for mean flow values and HW data for turbulence intensity in the wire disk, testing the pressure probes ability to accurately measure turbulence. Further analysis shows a cross-sectional wake comparison of the two disks for all three components of the mean flow, turbulence intensity, and Reynolds shear stresses in Cartesian coordinates, measured at $x = 4D$. Finally, the axial velocity component, turbulent kinetic energy(TKE) and Reynolds shear stress was compared for the two disks with turbine cross hot wire measurements by Eriksen and Krogstad (2017). It will be shown that the choice of actuator disk is of crucial importance when modeling wind turbine wakes.

3 Experimental setup

3.1 Wind tunnel specifications

The experiments were conducted in the wind tunnel at NTNU, Trondheim, Norway. It is a closed-loop tunnel with a test section of 2.71m x 1.81m x 11.15m corresponding to width, height, and length. To ensure spatially uniform inflow, a grid with solidity a of $\sigma = 35.4\%$, wire thickness $t_{grid} = 0.6mm$ and mesh length of $M_{grid} = 2.49mm$ was used. A similar grid with slightly coarses mesh was also used at the outlet. The background velocity and turbulence intensity was measured with the CP to $u_{inn} = 8.55m/s \pm 0.1m/s$, and $Ti = 0.86\% \pm 0.5$, respectivly, both at a 95% confidence interval.

3.2 The actuator disks

The two different disks used, had the same solidity($\sigma = 57\%$ and diameter ($D = 20cm$) giving equal Reynolds number (Re_D). The drag coefficient, C_D, (not shown) was measured on the force balance in the wind tunnel at 8 Reynolds number increments from $7x10^4$ to $3x10^5$ and showed Reynolds number independence. For the wire disk this was measured to $C_{D,WD} = 0.77 \pm 0.01$ and $C_{D,SD} = 0.82 \pm 0.01$ for the spider disk. Both disks were connected to a mast with $D_{mast}/D_{disk} = 0.05$. For the wire disk, this mast was glued on, while the spider disk was attached with a bearing in the center. The mast was further attached to a larger pole which was used to ensure no influence from the boundary layer in the wind tunnel on the disks. A helical coil was also used on the larger mast to avoid any vortex induced vibration from the mast to interfere with the measurements.

The wire disk(WD) was made from a mesh of woven steel wire and had a wire thickness 1mm and hole size of 2mm. The result was a disk that has a uniform force extraction being the physical equivalent of the simplest actuator disk. The spider web disk(SD) was created based on a design by Camp and Cal (2016). The disk had a thickness of 6.5 mm, and was axisymmetric with 30 columns of increasing hole size meant to mimic the decreasing blockage experience in wind turbines.

3.3 Cobra Probes

The measurements was conducted using a Turbulent Flow Instrumentation Cobra probe(CP) series 100 (TFI, 2019). It is a 4 hole pressure probe with a frequency response of 650 Hz under normal operating conditions. The technique uses a linearized frequency response that allows for measurements of mean flow values of in three dimensions along with turbulent fluctuating properties. The probes are calibrated by the manufacturer and match pressure relationship between the 4 holes voltage signal to the three velocity components u, v, w along with static pressure. For more information about this procedure see (Hooper and Musgrove, 1997).

The accuracy of the probe is calculated by Mühle (2018) to be around 5% for the mean values and 8% for the turbulent intensity.

For the present case, the time series voltage data was acquired and evaluated using MATLAB scripts acquired from the manufacturer (TFI, 2019). Sampling was taken at 10240 Hz using an oversampling rate of 8 to reduce aliasing. This resulted in time series data at 1280Hz with a digital filter at 50% of this. Total sampling time of 2 minutes was used. The measurements

Figure 1. Spider web disk to the left and wire mesh disk to the right. Both disks have a diameter of 20cm and where attached to a mast of $D_{mast}/D_{disk} = 0.05$

was taken in a cross sectional plane, normal to the mean flow direction at $x = 4D$. 663 sample points, Figure 2 were taken, at $y, z = \pm 1D$ In order to make the contour plots, evenly distributed points was needed and in the lower and upper vertical regions, linear interpolation in the horizontal direction was used.

3.4 Contributions of data

Kyrkjeboe (2019) measured the wake of the wire disk at $x = 4D$ using single hot wires. The same inlet and outlet passive wire grid setup were used to ensure uniform, low turbulence flow, but using a slightly lower inlet velocity ($u_\infty = 8m/s$ vs $u_\infty = 8.5m/s$).

Eriksen and Krogstad(2017) measured the wake of a rotating turbine using the NREL S826 airfoil. The free stream velocity was $u_\infty = 10m/s$ and background turbulence intensity was $Ti = 0.24\%$. The wind turbine had a drag coefficient of $C_D = 0.81$ (Bartl and Sætran, 2016b), and a diameter of $0.90m$ resulting in a blockage of 13%. Cross-hot wires were used to measure three components of the flow in the wake, giving output data on Reynolds shear stress' $\langle u'v' \rangle$ as well as all three normal stresses $\langle u'^2 \rangle, \langle v'^2 \rangle, \langle w'^2 \rangle$ which in the present case has been summed up to the turbulent kinetic energy eq. (1).
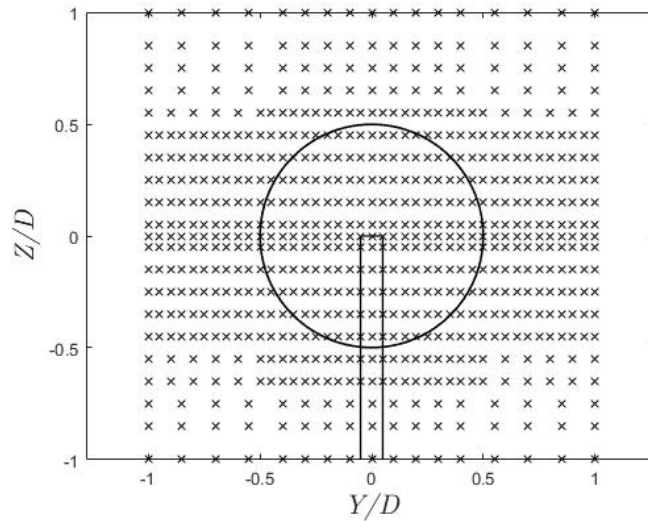
Figure 2. Position of the sample points, showing a total of 663 points.

4   Theory

In this paper Reynolds averaging was used with $u_i(t) = \langle u_i \rangle + u'_i$, where $\langle u_i \rangle$ is the mean value and u'_i is the fluctuating part of the velocity components in Cartesian coordinates. Right hand rule is used with X being down stream direction, y is the horizontal orthogonal and z is the vertical orthogonal direction corresponding to u,v,w respectively. From now $u_i(t) = u_i$ notation is used.

The Turbulent Kinetic Energy (TKE) is calculated as follows:

$$TKE = 0.5(\langle u'^2 \rangle + \langle v'^2 \rangle + \langle w'^2 \rangle) \tag{1}$$

This is known as a half the sum of the normal - diagonal Reynolds stresses ($\langle ui'uj' \rangle$) which from statistics are known as a samples variance. This describes the energy in the turbulent bursts in a given direction. The remaining elements of the Reynolds stress tensor are $\langle u'v' \rangle, \langle u'w' \rangle, \langle v'w' \rangle$ which is a measure of the direction of the turbulence. For computational models, the Reynolds stress tensor is usually modelled by the Boussinesq hypothesis (Schmitt, 2007) as:

$$\langle u_i u_j \rangle = \frac{2}{3} TKE \delta_{ij} - \nu_T \left(\frac{\partial u_i}{\partial x_j} + \frac{\partial u_j}{\partial x_i} \right) \tag{2}$$

where δ is the kroenicker delta which is zero for $i \neq j$. In the cases of $i = 1$ and $j = 2$ this can be simplified to $\langle u'v' \rangle = -\nu_T(\frac{\partial u}{\partial y})$ because $\frac{\partial u}{\partial y} >> \frac{\partial v}{\partial x}$.

Another method to calculate the turbulence is the turbulence intensity. This allows for a simple non dimensionless comparison of the strength of the turbulence in relations to the relative velocity in the respective location. The equation is defined:

$$Ti_i = \frac{\sqrt{\langle u_i'^2 \rangle}}{\langle U \rangle} \tag{3}$$

where U velocity is the total velocity calculated as $U = \sqrt{\langle u^2 \rangle + \langle v^2 \rangle + \langle w^2 \rangle}$. The total turbulence intensity is calculated by taking the mean of the three components:

$$Ti = (Ti_u + Ti_v + Ti_w)/3 \tag{4}$$

5 Results
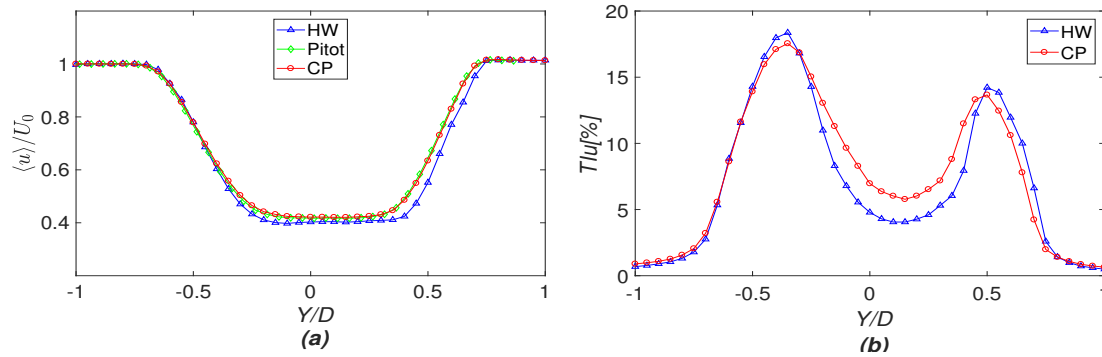
5.1 Validation of the Cobra Probes

Figure 3. Mean velocity (a) and turbulence intensity(b) measured at x = 4D behind the WD.

The Cobra probe(CP) has been compared with hot wire(HW) data acquired by Kyrkjeboe (2019) for mean flow and turbulence intensity and a pitot tube used in collaboration with the CP(for higher order moments see appendix). The measurements were taken at hub height($z/D = 0$), 4 diameters downstream of the disks which from Figure 4 shows to be in the upper parts of the wake. Meaning the wake profiles are sensitive to small differences in positioning of the measurement equipment in the vertical direction. Figure 3(a) shows the mean values normalized by the free stream velocity. The CP shows good agreement with the pitot tube, while the hot wire shows a lower deficit and some sidewash of the wake. The hot wire is calibrated against a pitot tube for mean values and therefore these differences are most likely caused by measuring different parts of the wake, either by different placement of the measurement equipment, or differences in downwash experienced at lower velocity. The effect of the latter part however, has not been tested.

Figure 3(b) shows the turbulence intensity comparison. The asymmetry in the peaks can be seen in both cases with a slightly lower value measured with the CP. With the differences shown in the mean values, one would expect differences to arise in the turbulence intensity as well. An important factor to take into account when measuring the turbulence is the effect of lower
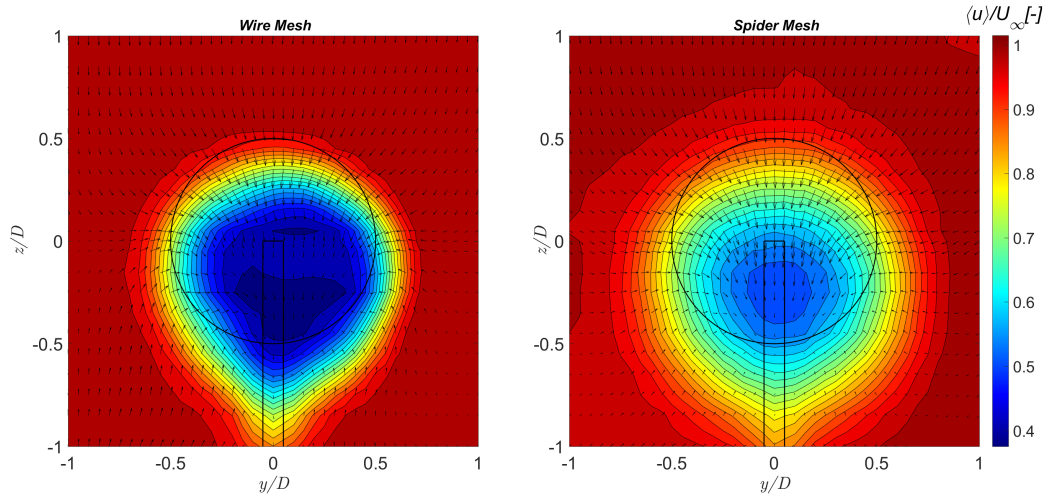
7

Figure 4. Mean values of the axial velocity component with velocity vectors for the two disks at $x = 4D$.

frequency response in the CP compared to the HW. The maximum frequency response of the CP is 640 Hz. From an analysis of the spectral density at the peak turbulence point(not shown here), the leftover turbulence energy in the hot wire measurements above this frequency is approximately 2% of the total turbulent energy. The biggest challenge for the CP rather is shown in the turbulence intensity measured in the center of the wake. At $\langle u \rangle = 3.5 m/s$ the pressure signal is less than 0.7% of the total capacity of this probe, meaning accurately measuring pressure variations, especially at lower scales becomes difficult.

Having seen the strong overlap of both mean values and turbulence intensity, and discussed the differences, these results prove the probes ability to accurately measure wake turbulence in a satisfying manner.

5.2 Cross-sectional wake field measurements

Figure 4 shows the axial velocity cross-section of both disks with velocity vectors. The first thing to notice is the downwash in both cases. As was mentioned when comparing the hot wire data, hub height (z/D = 0) is located in an area above the wake center, meaning the area is quite sensitive to small changes of measurement equipment. The mechanism of this downwash is illustrated by the velocity vectors from the planewise velocity components. A previous study by Pierella and Saetran (2017) showed how turbine tower interaction caused downwash that disappeared when a dummy tower was mirrored upwards. It can also be seen that the SD produces a wider and more symmetrical wake with a lower velocity deficit than is seen in the WD.

In Figure 5 the horizontal velocity components are shown. This shows the flow being directed towards the disks wake center. The magnitude is stronger in the SD case showing over 40% higher peak value compared to the WD. In addition, it shows more symmetry with a gradual shift from negative to positive when crossing the $y/D = 0$ line while the WD only shows this direction in the shear layer parts of the wake.
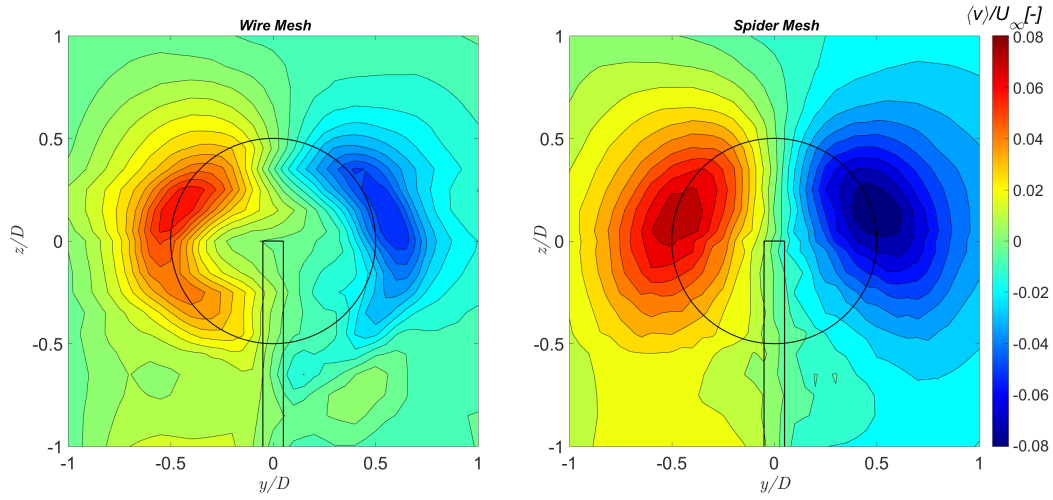
Figure 5. Mean values of the horizontal velocity component at $x = 4D$.
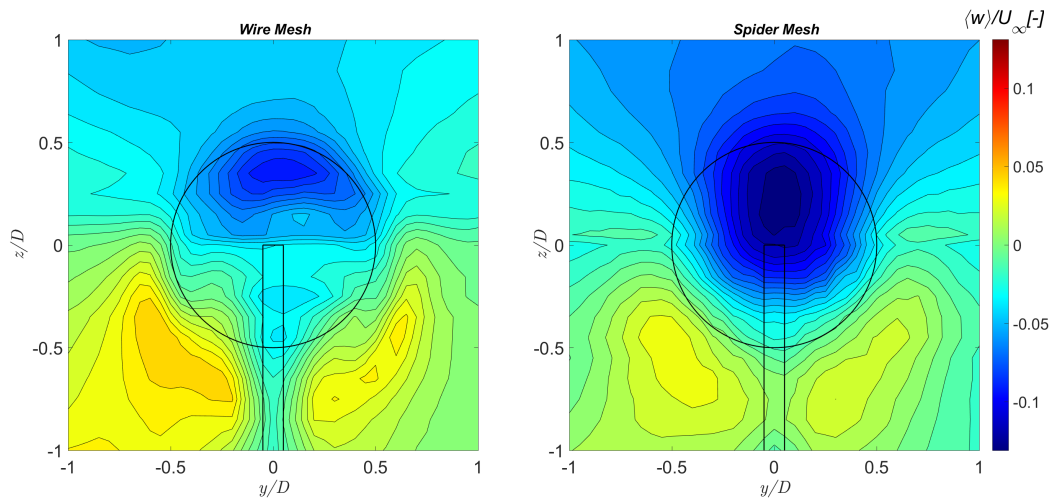

Figure 6. Mean values of the vertical velocity component at $x = 4D$.

Last of the mean values is the vertical velocity component seen in Figure 6. This shows the mechanism and strength of the downwash in the upper wake regions, with a negative component of 0.09 for the WD and 0.13 for the SD. Both disks also show

some upwash happening in the lower regions which are being masked by the mast. The magnitude of this upwash however is around 1/3 to 1/2 of the downwash magnitude.
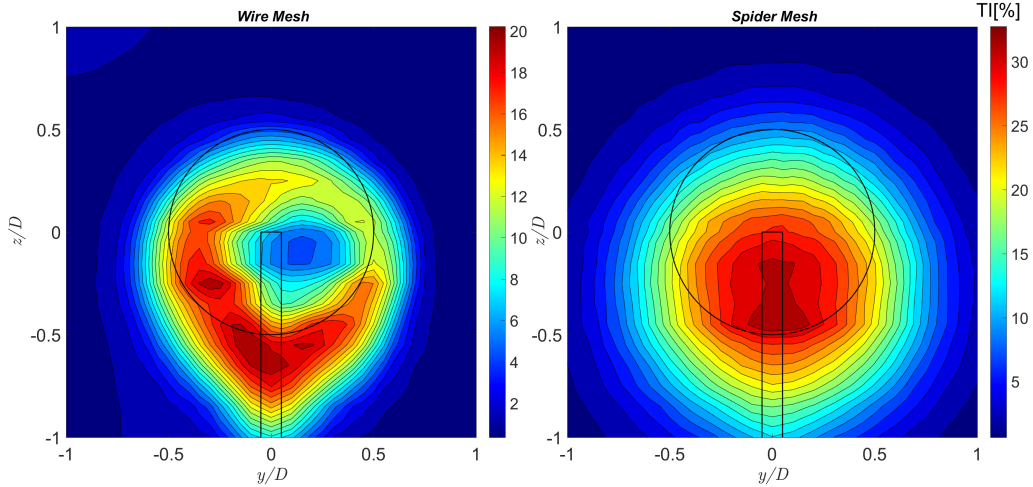

Figure 7. Turbulence intensity calculated by eq. (7) at $x = 4D$. Note the different scaling for the two plots.

The turbulence intensity can be seen in Figure 7. Different in color scaling is used for the two disks to avoid the SD scale masking the results of the WD. This shows that the SD has over 50% the magnitude of the WD, with its turbulence reaching the center of the wake. As has been seen in Figure 4 with a developed wake, the high turbulence intensity reaching the center of the disk shows the mechanism for this. With a high turbulence reaching the wake center highly increasing the wake mixing process. The WD has the turbulence located in the shear layer of the disk, the same area with the strongest velocity gradients seen in the axial flow component, Figure 4. A difference in the annular peaks can also be seen in the WD wake. The same was seen in the hot wire comparison Figure 3. Reasons for this asymmetry could be caused by local differences in background turbulence, inaccuracies in the tower-glue-attachment or small yaw-misalignment of the disk. These effects however are not certain.

In Figure 8 and Figure 9 the most important Reynolds shear stresses are shown, excluding $\langle v'w' \rangle$ because its low value. $\langle u'v' \rangle$ and $\langle u'w' \rangle$ are the stresses responsible for mixing of the flow from high velocity to low velocity in the horizontal and vertical direction respectively. From Boussinesq eq. (2) these are known to be negatively correlated with the planewise derivative of the axial velocity. Again we see that the magnitude of flow mixing is stronger in the SD case, with a fully developed shear turbulence at about twice the magnitude of the WD in both Figure 8, and Figure 9. Also, a stronger symmetry can be seen in the SD case. Comparing the two different Reynolds stresses shows that for both disks the strongest mixing is happening in the horizontal direction, with the vertical having a magnitude around two thirds of the horizontal. The stronger flow entrainment
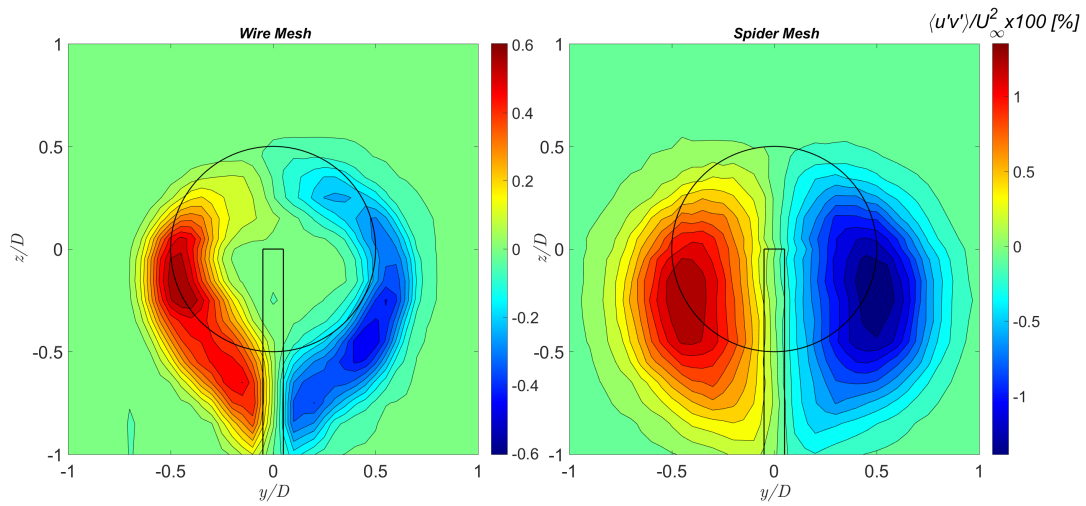
Figure 8. Normalized Reynolds Shear stresses in the horizontal direction. Note the different scaling.

from the sides could be attributed to the presence of the tower limiting flow from below. However, this does not explain the vertical shear stress in the top part of the wakes being equal the bottom part.
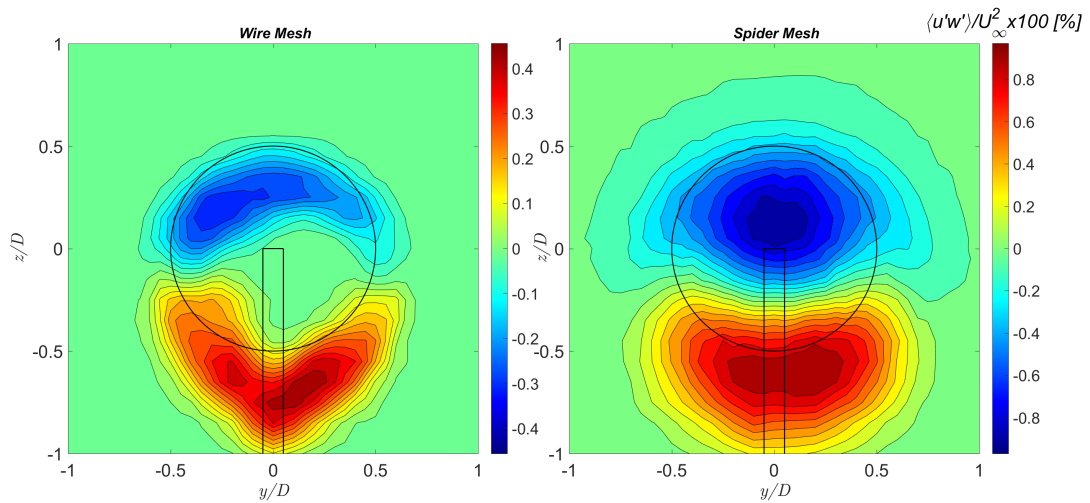

Figure 9. Normalized Reynolds shear stresses in the vertical direction. Note the different scaling.
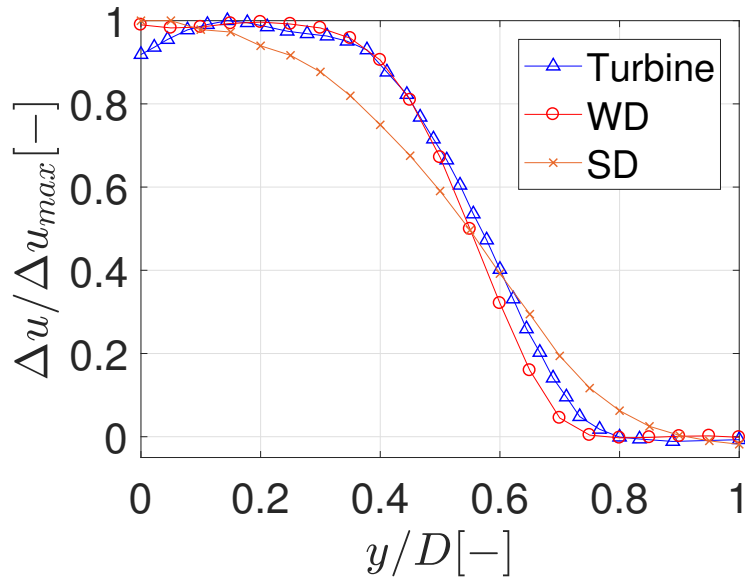
Figure 10. Comparison of the normalized axial velocity of the turbine (Eriksen and Åge Krogstad, 2017) and the two disks at the wake center, $x = 4D$. Normalization as $(u_\infty - \langle u \rangle)/(u_\infty - u_0)[-]$.

5.3 Turbine Disk Comparison

In this section, a comparison of the porous disk wakes with cross hot wire measurements conducted by Eriksen and Krogstad (2017). The turbine used had a diameter of 0.9m, using the NREL S826 airfoil. The hot wire measurements were taken at the half width of the wake at $x = 4D$ downstream. Because of the downwash experienced by the porous disk wakes the data was taken from the wake center (y/D = -0.15) and not at hub height, where the turbine measurements were done. In Figure 10 a normalized plot of the turbine disk axial velocity component is shown. The scaling is normalized so that the minimum wake velocity is equal to 1 and the free stream velocity is zero. The turbine has a blockage ratio of 13% which forces the surrounding freestream to take larger values than the inlet conditions. Therefore the turbine wake is normalized by its asymptotic wake free stream value ($u_\infty = 11.5m/s$) and not the inlet value ($u_\infty = 10m/s$). This is done because we are not interested in the blockage effect caused by the large turbine in the small tunnel. In the wake center, the effect of the tower nacelle can be seen in the turbine case where no energy extraction is done. In Aubruns (2013) comparison of disks and turbine wakes a courser mesh was used in the center to get this effect on the disk wake. Apart from this, the shape of the WD wake follows the turbine disk well, though the turbine shows a wider wake profile, which could be due to sidewash in the turbine case. The SD has a different velocity profile with a more Gaussian shape of the velocity causing a narrower profile in the center and wider profile in the wake ends.

In Figure 11 the horizontal Reynolds shear stress $\langle uv \rangle$ is shown to the left and the sum of the normal stresses to the right. The magnitude of the radial Reynold shear stress show good agreement for the WD and the turbine, with the turbine having a slightly wider and higher value. The SD shear stress profile is quite different than the turbine and WD, with about three times the magnitude going across an area from 0 to $1y/D$. The same trends seen in the $\langle u'v' \rangle$ plots were also seen for the TKE. The
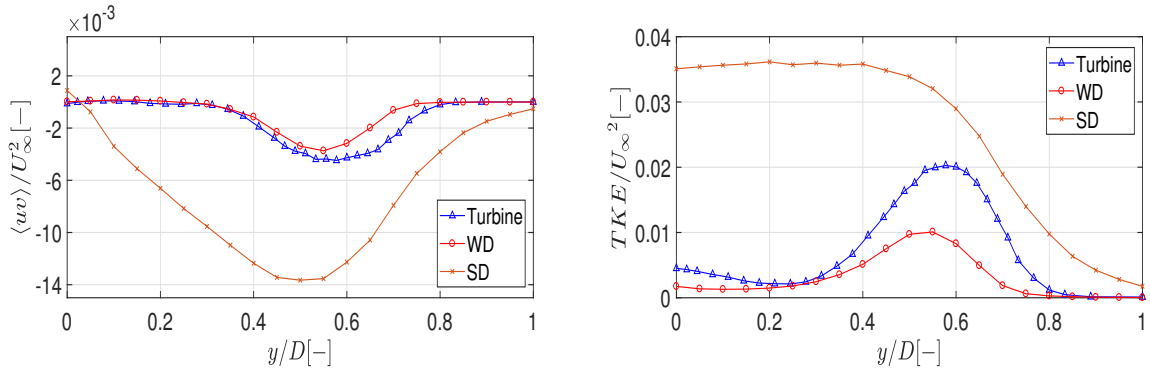
Figure 11. Comparison of the Reynolds shear stress and turbulent kinetic energy for the turbine (Eriksen and Åge Krogstad, 2017) and two disks at the wake center, $x = 4D$.

SD produces higher turbulence than the WD and the turbine, with the turbine and the WD having a peak in the shear layer of the wake. This causes the wake to regenerate much faster than for the turbine and wire disk.

6 Conclusion

Wake measurements of two actuator disks have been done and the wake was established in a plane $y, z = \pm 1D$ at $x = 4D$ downstream of the disks using Cobra probes. The cobra probe technique was compared against pitot tube and hot wire data for the mean flow values and hot wire data for turbulence intensity in the wake of the wire wake. The mean values showed overlap for the Cobra probe and pitot tube and followed closely for the hot wire data, which showed a slightly lower velocity in the center of the wake and some sidewash. Comparison of the turbulence intensity also showed good agreement. The Cobra probe showed slightly lower peak turbulence in the shear layer, and higher turbulence in the center of the wake. This wake center difference highlights a weakness of the pressure probes with higher inaccuracies experienced when sampling turbulence at a pressure 0.7% of the probes total range. However, these results show the ability of the Cobra probe to accurately measure turbulence in a satisfying manner.

Further, contours of the wake in a plane at 4 disk diameters downstream were shown for all three mean velocity components, as well as turbulence intensity and Reynolds shear stresses.

This showed that both disks experienced downwash, putting the wake center at a lower vertical position than the geographical center of the disks. For the uniformly meshed wire disk, the wake was undeveloped with a low wake center velocity and turbulence located in the shear layer. The spider disk showed a fully developed Gaussian wake with strong turbulence reaching the center of the wake.

The disks wake center were then comparison with cross-hot wire measurements of a wind turbine using the NREL S826 airfoil. This showed good overlap between the turbine and the wire disk, while large differences were seen in spider disk. The velocity shape of the wire disk showed similar shape as the turbine with the turbine having a slightly wider wake and lower

central deficit caused by the nacelle interference. The spider disk had a narrower profile in the center and wider in the wake end. The magnitude of the shear turbulence of $\langle u'v' \rangle$ and the TKE showed some slightly stronger values for the turbine than the disk, however this shows the potential of using uniform meshed wire disk to create wind turbine wakes, while the opposite is true for the spider disk that showed a different velocity profile and much higher turbulence magnitudes.

7 Appendix

7.1 Introduction higher order statistics

For Gaussian distributions, the probability density function(PDF) is fully determined by the first and second order statistical moments namely, mean value and standard deviation. However, not all PDFs have Gaussian distributions, and in these cases, higher order statistics involving skewness and kurtosis is needed. Schottler *et al.* (2018) measured the wake of two different wind turbines operating normal to the flow and with yaw misalignment. The use of first and second order statistical methods was extended using a two-point, fourth order moment showing velocity increment deviations from Gaussian distributions. This proved that the turbulence wake effects happened over a wider area than seen using only first and second order statistics. Study on porous disks by Cannon (1993) linked large scale turbulent structures, as helical vortex shedding, to disk porosity. Aubrun (2013) showed that in the far wake regions $x/D = 3$, wind turbine skewness and flatness could be reproduced by porous disks when compared with rotating turbines in high turbulent inlet conditions. At lower turbulent inlet conditions larger discrepancies were shown.

In the present case, the statistical moments are extended using third and fourth order statistics. The validity of the CP technique has been analyzed by comparing with HW data acquired by Kyrkjeboe (2019) at $x = 4D$ in the WD wake. Analysis of the PDFs in selected points has been shown and discussed. Lastly, the cross-sectional wake planes are shown for skewness and the two-point fourth order shape factor λ^2 revealing non-Gaussian velocity distributions in the wakes.

7.2 Higher order statistical theory

Higher order statistics of the 3rd and 4th order is the skewness and kurtosis of a sample distribution. The skewness is calculated as:

$$S(u_i') = \frac{\langle u_i'^3 \rangle}{\langle u_i'^2 \rangle^{3/2}} \tag{5}$$

This is a measure of the symmetry of the PDF. A PDF with negative skewness means more extreme events of negative value are more likely than of positive.

$$F(u_i') = \frac{\langle u_i'^4 \rangle}{\langle u_i'^2 \rangle^2} \tag{6}$$

A Gaussian PDF has a kurtosis, or flatness, equal to three, with higher flatness indicating a larger occurrence of extreme events than would be expected with a Gaussian distribution.

To get a deeper analysis of the disks wakes a two-point, 4th order statistical method is also used and calculated using a velocity increment. This gives an insight into turbulence that happens over a timescale associated with the incoming velocity and length scale of the disks. The method is the same as used in Schottler *et al.* (2018), based on Chillà *et al.* (1996). The velocity increment is calculated as:

$$u_\tau(t) = u(t) - u(t + \tau) \tag{7}$$

The physical intuition of this is that $|u_\tau(t)|$ is large when a large velocity change happens over a timescale of $t + \tau$. In this case, τ is calculated from the length scale D given as:

$$\tau = D/\langle u \rangle, \tag{8}$$

where D is the disk diameter and $\langle u \rangle = 8.5 m/s$ is the mean velocity in the free stream. The shape factor,λ^2 is calculated as:

$$\lambda^2(\tau) = \frac{ln(F(u_\tau)/3)}{4} \tag{9}$$

This is used to make a quantitative analysis of how the distribution $p(u_\tau)$ is. For Gaussian distributed PDFs, this becomes zero while for PDFs with heavy tails the value is increased. The increment flatness used is calculated as:

$$F(u_\tau) = \frac{\langle (u_\tau - \langle u_\tau \rangle)^4 \rangle}{\langle u_\tau^2 \rangle^2} \tag{10}$$

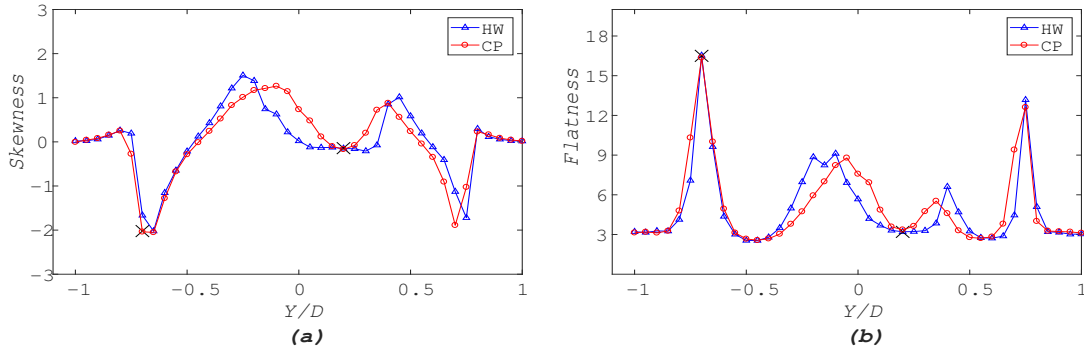## 7.3 Hot wire comparison

Figure 12. Skewness and kurtosis measured at hub height behind WD, comparison of HW, CP and pitot tube for mean value only. HW data from Kyrkjeboe (2019)

In Figure 12 the comparison of skewness(a) and flatness(b) between the HW and CP is shown. As discussed in section 5.1 the differences in measured mean values means one can expect differences in the other moments as well. Here the CP captures the extrema points well in both cases, with differences in the center. This central difference is likely enhanced by the challenge of the probe to capture accurately fluctuations at this small scale. However, this shows the capability of the probes to capture even fluctuations of higher order and giving values to an an acceptable rate.

For more information about the differences between the CP and HW, plots of the PDF from the marked points, seen in Figure 12, are shown in Figure 13. For the case without the increment, the PDF shows the for $y = -0.7D$ the area with negative skewness with tails towards the negative side, indicating the wind having the tendency to have more extreme negative values. While the PDFs at $y = 0.2D$ shows a more Gaussian shape which is much less likely to have occurrences of extreme events. An important difference between the HW and CP is the sample amount. The HW captured a total of 9,000,000 samples
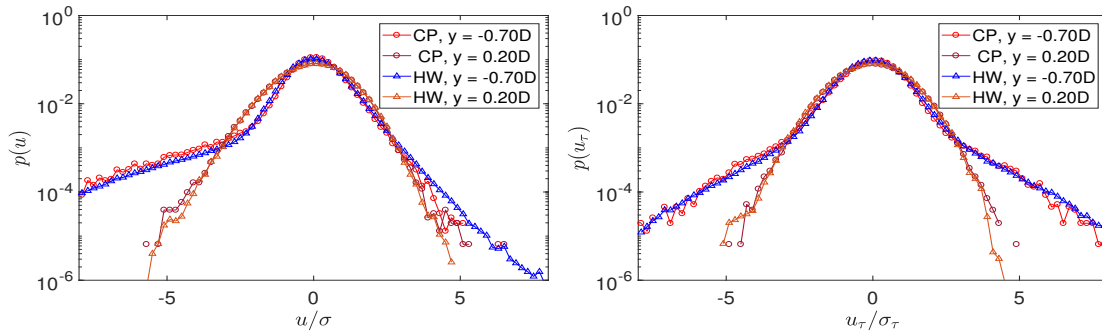
Figure 13. Probability density functions for selected points, first the normal time series data PDF is shown then as a function of the velocity increment calculations. HW data from Kyrkjeboe (2019)

over a time of 5 minutes, while the CP had an output at 153,600 samples which is almost 60 times less. At the tails of the PDF in the maximum kurtosis and skewness, each sample increment point has around 15 occurrences (calculated as $153,500 * 10^{-4} = 15.36$), which shows that the convergence of these extreme events is much less for the CP than for the HW. This obviously increases the uncertainty of the CP measurements.

Looking at the time increment PDF, the same can be seen. This shows changes of the wind happening over a given time scale associated with the inlet velocity and size of the disks. In $y = 0.7D$, at the tails, between 1 and 15 measurements are recorded in each bin increment, which is seen with the lines being pointier. However, the general profile is seen with a narrower profile in the center with stronger tails showing the PDF to take large values which would not happen if the turbulence showed fully Gaussian tendencies.

These comparisons show that Cobra probes can be used to capture data usable to calculate even higher order moments accurately. Even though the lack of data points increases the uncertainty of the calculated value, the probes capture the trends well and are able to pick up the signals of large scale rapid changing turbulence.

7.4 Cross sectional wake fields

In Figure 14 the skewness wake is shown for the two disks. In both cases the skewness has a negative annular layer around the wakes showing how the flow tends to take larger negative values. The magnitude of this is much larger in the case of the SD and it happens over a larger and wider width as well. Lastly in Figure 15, λ^2 is calculated. This has a zero value for Gaussian shaped PDFs. In both cases a annular ring surrounding the area with wake velocity deficit is seen. The magnitude is about three times as high in the SD case compared to the WD, and also showing presence of these large turbulent structures over a larger radial area. Similar findings was seen by Schottler *et al.* (2018) on two model turbines at $x = 6D$. The magnitude in these cases however was around 0.2 - 0.3, showing a closer value to the WD than the SD. These results show that the wake effects happends over a larger area than seen when only using first and second order statistics.
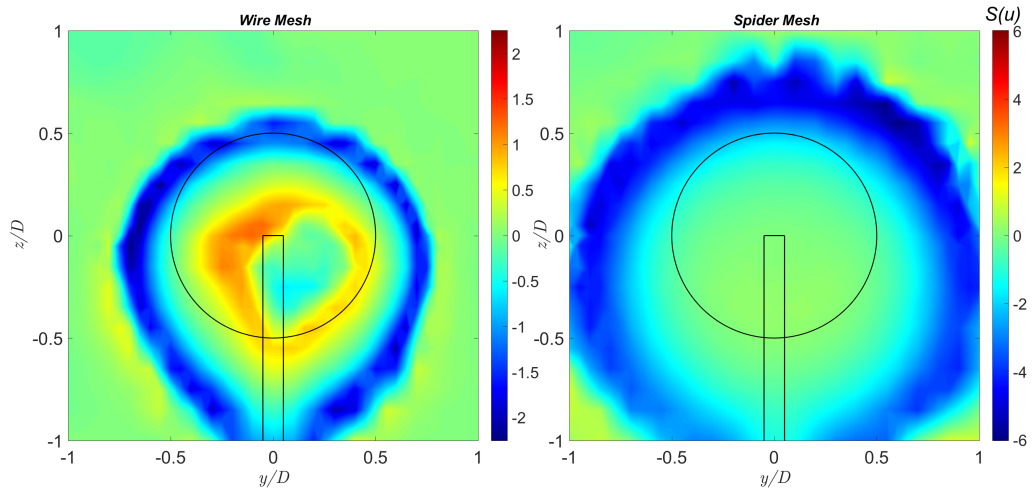
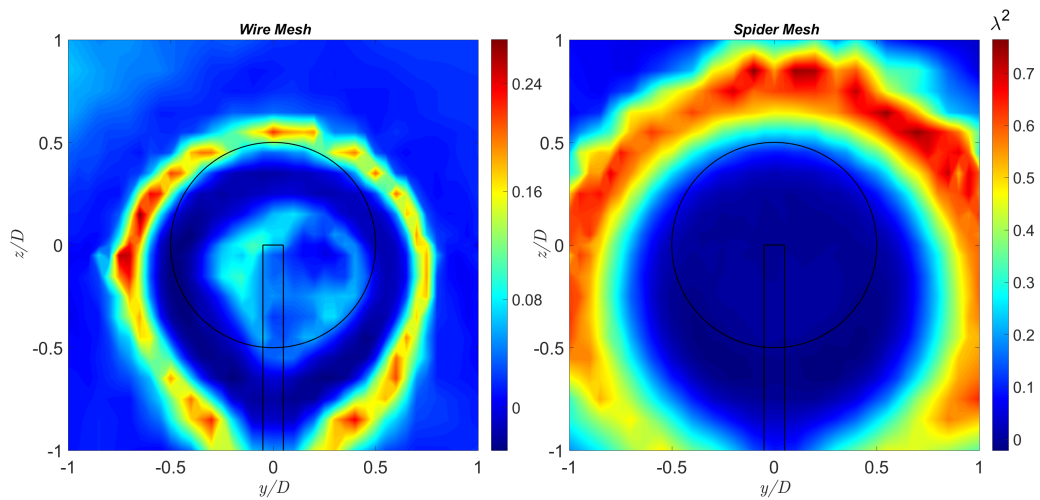**Figure 14.** Skewness factor in the wake of the two disks.Note the different scaling.

Figure 15. Shape factor λ^2 in the wake of the two disks showing annular area with heavy tails in the velocity increment PDF, see eq. (15). Note the different scaling.

7.5 Conclusion

Higher order statistics of skewness and kurtosis were compared with HW measurements and showed good agreement. Analysis of the probability density functions of selected points showed the effect of fewer samples, by a magnitude of 60, put larger uncertainty on the specific shape of the distribution, however, the trend was captured well. The skewness analysis showed how the PDF tended to have negative tails in both cases in an area around surrounding the wakes with magnitudes about 3 times the size for the spider disk compared to the wire disk. This also happened over a larger physical area for the spider mesh. Using the shape factor λ^2 showed likewise large structures in the wakes of both disks surrounding the velocity deficit area. This has previously been linked to vortex shedding mechanism for porous disks over a given solidity. The spider disk produced a higher magnitude by the order of 3 over a larger area in comparison to the wire disk which had a value close to that seen in model turbines. This shows the ability for uniformly meshed wire disk to be used in capturing higher order moments, while the disk using a radially distributed blockage, overproduces these components in comparison. It also shows that these large scale turbulent structures occurs in non rotating disks, and that the wake effects happens over a larger radial area than seen using first and second order statistics.

References

Getting started - TFI 100 used guide, https://www.turbulentflow.com.au/Downloads/Getting%20Started%20-%20Cobra%20Probe.pdf, 2019.

Aubrun, S.: Modelling Wind Turbine Wakes with a Porosity Concept, https://doi.org/10.1007/978-3-540-33866-6_49, 2007.

Aubrun, S., Loyer, S., Hancock, P., and Hayden, P.: Wind turbine wake properties: Comparison between a non-rotating simplified wind turbine model and a rotating model, JOURNAL OF WIND ENGINEERING AND INDUSTRIAL AERODYNAMICS, 120, 1 – 8, https://doi.org/10.1016/j.jweia.2013.06.007, http://epubs.surrey.ac.uk/809002/, © 2013. This manuscript version is made available under the CC-BY-NC-ND 4.0 license http://creativecommons.org/licenses/by-nc-nd/4.0/, 2013.

Barthelmie, R. J., Pryor, S. C., Frandsen, S. T., Hansen, K. S., Schepers, J. G., Rados, K., Schlez, W., Neubert, A., Jensen, L. E., and Neckelmann, S.: Quantifying the Impact of Wind Turbine Wakes on Power Output at Offshore Wind Farms, Journal of Atmospheric and Oceanic Technology, 27, 1302–1317, https://doi.org/10.1175/2010JTECHA1398.1, https://doi.org/10.1175/2010JTECHA1398.1, 2010.

Bartl, J. and Sætran, L.: Blind test comparison of the performance and wake flow between two in-line wind turbines exposed to different atmospheric inflow conditions, Wind Energy Science Discussions, pp. 1–31, https://doi.org/10.5194/wes-2016-31, 2016a.

Bartl, J. and Sætran, L.: Experimental testing of axial induction based control strategies for wake control and wind farm optimization, Journal of Physics: Conference Series, 753, 032 035, https://doi.org/10.1088/1742-6596/753/3/032035, 2016b.

Bastankhah, M. and Porté-Agel, F.: A new analytical model for wind-turbine wakes, Renewable Energy, 70, 116 – 123, https://doi.org/https://doi.org/10.1016/j.renene.2014.01.002, http://www.sciencedirect.com/science/article/pii/S0960148114000317, special issue on aerodynamics of offshore wind energy systems and wakes, 2014.

Cannon, S., Champagne, F., and Glezer, A.: Observations of large-scale structures in wakes behind axisymmetric bodies, Experiments in Fluids, 14, 447–450, https://doi.org/10.1007/BF00190199, https://doi.org/10.1007/BF00190199, 1993.

ChillĂ , F., Peinke, J., and Castaing, B.: Multiplicative Process in Turbulent Velocity Statistics: A Simplified Analysis, http://dx.doi.org/10.1051/jp2:1996191, 6, https://doi.org/10.1051/jp2:1996191, 1996.

Crespo, A., Hernández, J., and ST, F.: Survey of modelling methods for wakes and wind farms, Wind Energy, 2, 1–24, https://doi.org/10.1002/(SICI)1099-1824(199901/03)2:13.3.CO;2-Z, 1999.

Eriksen, P. E. and Åge Krogstad, P.: Development of coherent motion in the wake of a model wind turbine, Renewable Energy, 108, 449 – 460, https://doi.org/https://doi.org/10.1016/j.renene.2017.02.031, http://www.sciencedirect.com/science/article/pii/S0960148117301179, 2017.

H. Camp, E. and Cal, R. B.: Mean kinetic energy transport and event classification in a model wind turbine array versus an array of porous disks: Energy budget and octant analysis, Physical Review Fluids, 1, 044 404, https://doi.org/10.1103/PhysRevFluids.1.044404, 2016.

Hansen, M.: Aerodynamics of wind turbines, Second edition, Aerodynamics of Wind Turbines, Second Edition, pp. 1–181, https://doi.org/10.4324/9781849770408, 2013.

Hooper, J. and Musgrove, A.: Reynolds stress, mean velocity, and dynamic static pressure measurement by a four-hole pressure probe, Experimental Thermal and Fluid Science, 15, 375 – 383, https://doi.org/https://doi.org/10.1016/S0894-1777(97)00005-8, http://www.sciencedirect.com/science/article/pii/S0894177797000058, 1997.

Jensen, N.: A note on wind generator interaction, Risø National Laboratory, 1983.

Kermani, N. A., Andersen, S., Sørensen, J., and Shen, W.: Analysis of turbulent wake behind a wind turbine, 2013.

Kyrkjeboe, M.: High-order statistics of model wind turbine and actuator disk wakes, 2019.

Lignarolo, L., Ragni, D., Ferreira, C., and van Bussel, G.: Turbulent mixing in wind turbine and actuator disc wakes: An experimental analysis, 33rd Wind Energy Symposium, 2015.

Mikkelsen, R.: Actuator Disc Methods Applied To Wind Turbines, 2003.

Mühle, F.: An experimental study on rotor-wake interactions of wind turbines, Ph.D. thesis, 2018.

Pierella, F. and Sætran, L.: Wind tunnel investigation on the effect of the turbine tower on wind turbines wake symmetry: Experiments on wind turbine wake symmetry, Wind Energy, https://doi.org/10.1002/we.2120, 2017.

Schmitt, F. G.: About Boussinesq's turbulent viscosity hypothesis: historical remarks and a direct evaluation of its validity, Comptes Rendus Mécanique, 335, 617 – 627, https://doi.org/https://doi.org/10.1016/j.crme.2007.08.004, http://www.sciencedirect.com/science/article/pii/S1631072107001386, joseph Boussinesq, a Scientist of bygone days and present times, 2007.

Schottler, J., Bartl, J., Mühle, F., Sætran, L., Peinke, J., and Hölling, M.: Wind tunnel experiments on wind turbine wakes in yaw: redefining the wake width, Wind Energy Science, 3, 257–273, https://doi.org/10.5194/wes-3-257-2018, https://www.wind-energ-sci.net/3/257/2018/, 2018.

Stergiannis, N., Beeck, J., and Runacres, M.: Full HAWT rotor CFD simulations using different RANS turbulence models compared with actuator disk and experimental measurements, Wind Energy Science, https://doi.org/10.5194/wes-2017-6, 2017.

Tian, W., Ozbay, A., and Hu, H.: Effects of incoming surface wind conditions on the wake characteristics and dynamic wind loads acting on a wind turbine model, Physics of Fluids, 26, 125 108, https://doi.org/10.1063/1.4904375, https://doi.org/10.1063/1.4904375, 2014.

Vermeer, L., Sørensen, J., and Crespo, A.: Wind turbine wake aerodynamics, Progress in Aerospace Sciences, 39, 467 – 510, https://doi.org/https://doi.org/10.1016/S0376-0421(03)00078-2, http://www.sciencedirect.com/science/article/pii/S0376042103000782, 2003.
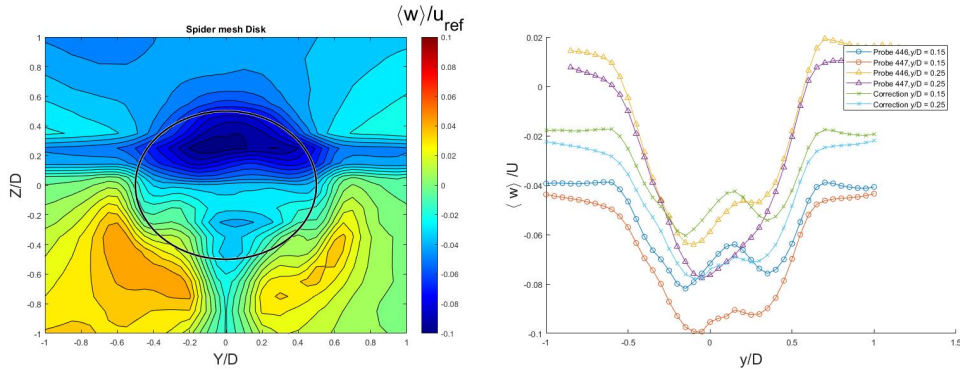
Figure 11. Data correction done by averaging the value of the two probes. Left figure is without correction, Figure 6 is with the right hand side correction.

Data correction

Figure 11 shows a calibration of two data lines in the vertical velocity component on the right hand side. The measurements was done using probe 446 while probe 447 was there as backup. The two lines revealed in the profile unphysical velocity gradients, likely induced by the attempt to keep the probes parallell to the flow direction when conducting the measurements. Therefore an averaging of the two probes was used to create the plots seen in Figure 6.

Unit: *Department of Energy and Process Engineering*   **Date: 10.06.2019**

Line manager:

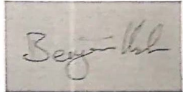**Participants in the identification process** (including their function): **Benjamin Karlsen**

Short description of the main activity/main process: Master project for student in the NTNU wind tunnel. Project title. Cross sectional wake measurements of Actuator disks.

Is the project work purely theoretical? (YES/NO):NO   *Answer "YES" implies that supervisor is assured that no activities*
requiring risk assessment are involved in the work. If YES, briefly describe the activities below. The risk assessment form need not be filled out.

Signatures: *Responsible supervisor:*   *Student:*   Benjamin Karlsen

ID nr.	Activity/process	Responsible person	Existing documentation	Existing safety measures	Laws, regulations etc.	Comment
4871 42	Wind tunnel work	Benjamin Karlsen				

	Risk assessment		Prepared by	Number	Date	
			HSE section	HMSRV2603E	04.02.2011	
			Approved by		Replaces	
			The Rector		01.12.2006	

Unit: *Department of Energy and Process Engineering*

Date:

Line manager:

Participants in the identification process (including their function): **Benjamin Karlsen, student**

Short description of the main activity/main process: Master project for student xx. Project title.

Signatures: *Responsible supervisor:*   *Student:* Benjamin Karlsen

Activity from the identification process form	Potential undesirable incident/strain	Likelihood: Likelihood (1-5)	Consequence: Human (A-E)	Environment (A-E)	Economy/ material (A-E)	Risk Value (human)	Comments/status Suggested measures
Wind tunnel work	Hitting head	5	A	A	A	A	
	Object hitting from high wind flow	2	A	A	A	A	

Likelihood, e.g.:
1. Minimal
2. Low
3. Medium

Consequence, e.g.:
A. Safe
B. Relatively safe
C. Dangerous

Risk value (each one to be estimated separately):
Human = Likelihood x Human Consequence
Environmental = Likelihood x Environmental consequence
Financial/material = Likelihood x Consequence for Economy/materiel

4. High   D. Critical
5. Very high   E. Very critical

Potential undesirable incident/strain

Identify possible incidents and conditions that may lead to situations that pose a hazard to people, the environment and any materiel/equipment involved.

Criteria for the assessment of likelihood and consequence in relation to fieldwork

Each activity is assessed according to a worst-case scenario. Likelihood and consequence are to be assessed separately for each potential undesirable incident. Before starting on the quantification, the participants should agree what they understand by the assessment criteria:

Likelihood

Minimal 1	Low 2	Medium 3	High 4	Very high 5
Once every 50 years or less	Once every 10 years or less	Once a year or less	Once a month or less	Once a week

Consequence

Grading	Human	Environment	Financial/material
E Very critical	May produce fatality/ies	Very prolonged, non-reversible damage	Shutdown of work >1 year.
D Critical	Permanent injury, may produce serious serious health damage/sickness	Prolonged damage. Long recovery time.	Shutdown of work 0.5-1 year.
C Dangerous	Serious personal injury	Minor damage. Long recovery time	Shutdown of work < 1 month
B Relatively safe	Injury that requires medical treatment	Minor damage. Short recovery time	Shutdown of work < 1week
A Safe	Injury that requires first aid	Insignificant damage. Short recovery time	Shutdown of work < 1day

The unit makes its own decision as to whether opting to fill in or not consequences for economy/materiel, for example if the unit is going to use particularly valuable equipment. It is up to the individual unit to choose the assessment criteria for this column.

Risk = Likelihood x Consequence

Please calculate the risk value for "Human", "Environment" and, if chosen, "Economy/materiel", separately.

About the column "Comments/status, suggested preventative and corrective measures":

NTNU		Risk matrix	prepared by HSE Section	Number HMSRV2604	Date 8 March 2010
[logo]			approved by Rector	Page 4 of 4	Replaces 9 February 2010
HSE/KS					

MATRIX FOR RISK ASSESSMENTS at NTNU

CONSEQUENCE	Extremely serious	E1	E2	E3	E4	E5
	Serious	D1	D2	D3	D4	D5
	Moderate	C1	C2	C3	C4	C5
	Minor	B1	B2	B3	B4	B5
	Not significant	A1	A2	A3	A4	A5
		Very low	Low	Medium	High	Very high
		LIKELIHOOD				

Principle for acceptance criteria. Explanation of the colours used in the risk matrix.

Colour		Description
Red		Unacceptable risk. Measures must be taken to reduce the risk.
Yellow		Assessment range. Measures must be considered.
Green		Acceptable risk Measures can be considered based on other considerations.

NTNU	Risk assessment	Prepared by	Number	Date
		HSE section	HMSRV2603E	04 02 2011
		Approved by		Replaces
HSE/KS		The Rector		01 12 2006

Measures can impact on both likelihood and consequences. Prioritise measures that can prevent the incident from occurring; in other words, likelihood-reducing measures are to be prioritised above greater emergency preparedness, i.e. consequence-reducing measures.